ISSN 3110-0635
https://doi.org/10.61401/rmaps.v4i1.760

Volume 4 Number 1, 2027
Review of Multidisciplinary Academic and Practice Studies

Summability-based Remaining Useful Life Estimation for Industrial Equipment

Avishek Shah[1*], Prem Kumar Nayak[2], Suresh Kumar Sahani[3]
Rajarshi Janak University, Janakpurdham, Nepal[1,2,3]
avishekshah@rju.edu.np[1*], premnayak6511@gmail.com[2], sureshsahani@rju.edu.np[3]

ARTICLE INFO

Received: 17 September 2026;
Revised: 4 October 2026;
Revised: 26 October 2026;
Accepted: 5 November 2026;
Volume 4, Number 1
2027, pp 17-39
https://doi.org/10.61401/rmaps.v4i1.760

Corresponding author:
Avishek Shah
Rajarshi Janak University, Janakpurdham, Nepal
E-mail: avishekshah@rju.edu.np

ABSTRACT

Purpose: This study develops a mathematically explicit summability-assisted framework for Remaining Useful Life (RUL) estimation, in which causal weighted means stabilize noisy degradation indicators before a prognostic model estimates RUL.
Methodology: Moving, Cesàro-type and exponential means are formulated as normalized causal weighted means, and their variance, bias and lag are derived. A threshold-crossing model maps the smoothed index to RUL with delta-method uncertainty. The framework is illustrated with a synthetic motor-driven pump, a synthetic replica of the NASA/IMS bearing record and a Monte Carlo experiment.
Results: In the pump example, a smoothed index of 0.723, a threshold of 1.00 and a slope of 0.0045 per hour gave an RUL of about 61.6 hours. Over 2,000 Monte Carlo runs, the first alarm of the raw feature was false in 78.2% of runs, against 0.6% for a 15-point moving mean and 2.0% for an exponential mean. Conclusions: Summability is a low-cost, interpretable preprocessing option when noise obscures slow degradation, but it can delay warnings and must be validated against baselines.
Limitations: All numerical examples are synthetic or simulated.
Contributions: The study provides equations, an algorithm and a validation protocol linking classical summability to prognostics.

Keywords: *Cesàro Mean, Exponential Weighting, Predictive Maintenance, Remaining Useful Life, Summability*

How to Cite: Shah, A., Nayak, P. K., & Sahani, S. K. (2027). Summability-based Remaining Useful Life Estimation for Industrial Equipment. *Review of Multidisciplinary Academic and Practice Studies*, 4(1), 17-39.

1. Introduction

Industrial maintenance has moved from fixed calendar intervals toward condition-based and predictive strategies. In a condition-based workflow, measurements indicate whether a component is healthy, degrading or approaching an operational limit, and Remaining Useful Life (RUL) expresses the predicted time or number of cycles until a defined end point such as a failure threshold, an inspection limit or a performance constraint. RUL is therefore not an intrinsic number, because it depends on the failure definition, operating duty, maintenance policy and uncertainty about future loads (Jardine, Lin, & Banjevic, 2006; Si, Wang, Hu, & Zhou, 2011; Zio, 2022).

A central obstacle is that degradation evidence is often obscured by measurement variability. A pump's vibration may rise during a valve transition, a compressor's temperature may change with the ambient conditions, and a bearing signal may include impacts unrelated to wear (Guo, Li, & Wan, 2023). Feeding every raw point into a prognostic model can produce unstable health indicators and erratic RUL trajectories, yet aggressive smoothing can hide abrupt fault onset and delay a warning. The mathematical problem is a balance between variance reduction, responsiveness, causal implementation and preservation of prognostic information.

Summability theory studies transformations of sequences, including arithmetic means of partial sums and weighted averaging (Buntinas, 2022; Hardy, 1949). Here, "summability-based" is used in a bounded sense, meaning that a sequence of recent sensor-derived features is transformed by a causal, normalized averaging operator before modelling, without implying that the signal is divergent. Recent work has applied Borel and Nörlund methods to Fourier series , to the approximation of signals through derived, Legendre and double Fourier series and to almost monotone sequences in ultraspherical, double Fourier and Legendre series (Pokharel, Pahari, & Sahani, 2023; Sahani, Mishra, & Rathour, 2022; Sahani et al., 2022; Sahani, & Mishra, 2021; Sahani and Mishra, 2021; Sahani, & Mishra, 2023). Summation methods for divergent series have been reviewed, Abel and Cesàro summability have been related in the interval-valued setting, and classical summability has been used to regularize divergent series in reliability and engineering systems (Sahani et al., 2022; Sahani and Mishra, 2021; Kartal, 2026; Chagas, & Lopes, 2021).

The study asks which summability operators suit noisy degradation features, how the smoothed trajectory can be converted into an interpretable RUL estimate, how latency, uncertainty and regime shifts should be handled so that smoothing does not create false confidence, and what evidence would establish benefit on real equipment. Its contributions are a causal weighted-mean formulation linking summability to feature stabilization, a degradation-rate and threshold-crossing RUL model with explicit assumptions, a hybrid architecture that keeps smoothing, prognosis, calibration and decisions separate, a worked industrial example with clearly labelled synthetic values, and an evaluation checklist. For safety-critical assets, an RUL model supports but does not replace inspection, protection systems or engineering judgement.

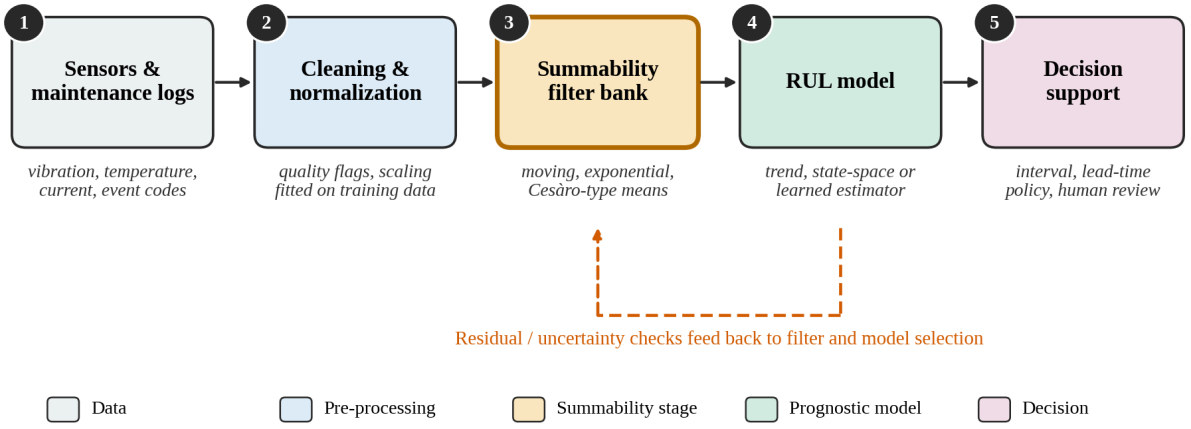


Figure 1. Proposed summability-assisted RUL architecture

Figure 1 shows the proposed architecture in five stages. Sensor and maintenance logs pass through cleaning and normalization, a summability filter bank, an RUL model and decision support. A dashed path carries residual and uncertainty checks back to the filter and model selection. The legend distinguishes data, preprocessing, the summability stage, the prognostic model and the decision, and the feedback path represents monitoring and revision rather than automatic closed-loop control.

2. Literature Review

2.1 RUL Estimation Families

Prognostics methods are commonly grouped into physics-based, data-driven and hybrid approaches (Jardine, Lin, & Banjevic, 2006; Si, Wang, Hu, & Zhou, 2011). Physics-based methods describe degradation through crack growth, fatigue or chemical ageing and can extrapolate when the mechanism is known, but their parameters are hard to identify in complex plant equipment, especially when operation and maintenance both shift failure behavior (Hu, Yang, Chen, Wu, & Xie, 2021). Data-driven methods learn the relation between sensor history and observed life and can represent nonlinear interactions, but they depend on representative run-to-failure histories and careful control of leakage. Zio (2022) notes a persistent gap between prognostics research and industrial practice, and multi-component systems add further complexity (Nguyen, Medjaher, & Gogu, 2022).

Deep learning has broadened RUL modelling through recurrent, convolutional, attention-based and probabilistic models (Wu, Wu, Tan, & Xu, 2024). Interval prediction matters because a point estimate does not show whether a prediction is reliable, and recent studies quantify RUL uncertainty with multi-distribution fusion, Bayesian active learning that reduces labelling needs and two-phase networks that identify degradation stages before Bayesian prediction (Bai, Noman, Feng, Peng, & Li, 2023; Chen, He, Hu, Yu, & Zhang, 2025; Zhan, Kong, Wang, Jin, & Xu, 2024; Zhu, Chen, Peng, & Ye, 2022). For bearings, impulse-driven health indicators (Guo, Li, & Wan, 2023) and implicit Kalman filtering with adaptive detection of stage transitions improve prediction stability (Li, Fu, & Li, 2025; Li, Wei, He, Yang, & Meng, 2023). These works motivate assessing preprocessing by calibration, timeliness and operational consequence as well as point accuracy.

2.2 Summability, Smoothing and Monitoring

For a sequence $x1, x2, \ldots$, Cesàro summability forms arithmetic means of partial sums, and closely related moving or cumulative averages reduce sensitivity to individual observations (Buntinas, 2022; Hardy, 1949). General matrix methods write transformed values as weighted sums, and conditions on the weights determine whether constants and ordinary limits are preserved. A finite-window causal filter is a finite weighted mean, and exponential smoothing assigns geometrically decreasing weights. Statistical monitoring offers a related view, since Exponentially Weighted Moving Average (EWMA) charts have been designed for time between events, for shifted exponential parameters and for bivariate Weibull data, while Cumulative Sum (CUSUM) methods locate change points in pump degradation (Chen, He, Hu, Yu, & Zhang, 2025; Xie, Castagliola, Qiao, Hu, & Sun, 2022; Baranwal, Kumar, Chatterjee, & Koukouvinos, 2025Li, Fu, & Li, 2025).

The connection should not be overstated. In predictive maintenance the target is a finite, nonstationary sensor sequence rather than a divergent series, and summability supplies a disciplined language for weight normalization, regularity and stability without identifying a failure mechanism. Benchmark data support fair comparison, including the simulated the National Aeronautics and Space Administration Commercial Modular Aero-Propulsion System Simulation (NASA C-MAPSS) turbofan data, the NASA/IMS bearing run-to-failure record, the Platform for Prognostics and Health Management of Rotating Machinery (PRONOSTIA) bearing platform and NASA battery data, but none replaces validation on the target asset. Table 1 summarizes the main modelling families and the role of summability in each (Goebel et al., 2008; Qiu et al., 2006; Nectoux et al., 2012).

Table 1. Main RUL modelling families and the role of summability

Family	Strength	Common weakness	Role of summability
Physics-based	Mechanism-level interpretation	Parameter identification and model mismatch	Stabilize measured inputs; preserve physical state equations

Family	Strength	Common weakness	Role of summability
Classical statistical	Transparent trends and survival assumptions	Limited nonlinear representation	Smooth features before trend/rate estimation
Machine learning	Flexible feature-to-RUL mapping	Data dependence and drift sensitivity	Reduce transient noise while retaining causal history
Deep learning	Learns temporal representations	Opaque failure modes; calibration challenges	Optional front-end filter or differentiable weighted aggregation
Hybrid prognostics	Combines physical and data evidence	Integration and validation complexity	Provide stable sensor features to a constrained model

Table 1 lists five families with their strength, common weakness and the role of summability. Physics-based models offer mechanism-level interpretation, and summability stabilizes their measured inputs without altering the state equations. Classical statistical and machine learning models gain smoother features before trend or rate estimation, and deep learning can use summability as an optional front-end filter. Hybrid prognostics combine physical and data evidence, and summability provides them with stable inputs to a constrained model.

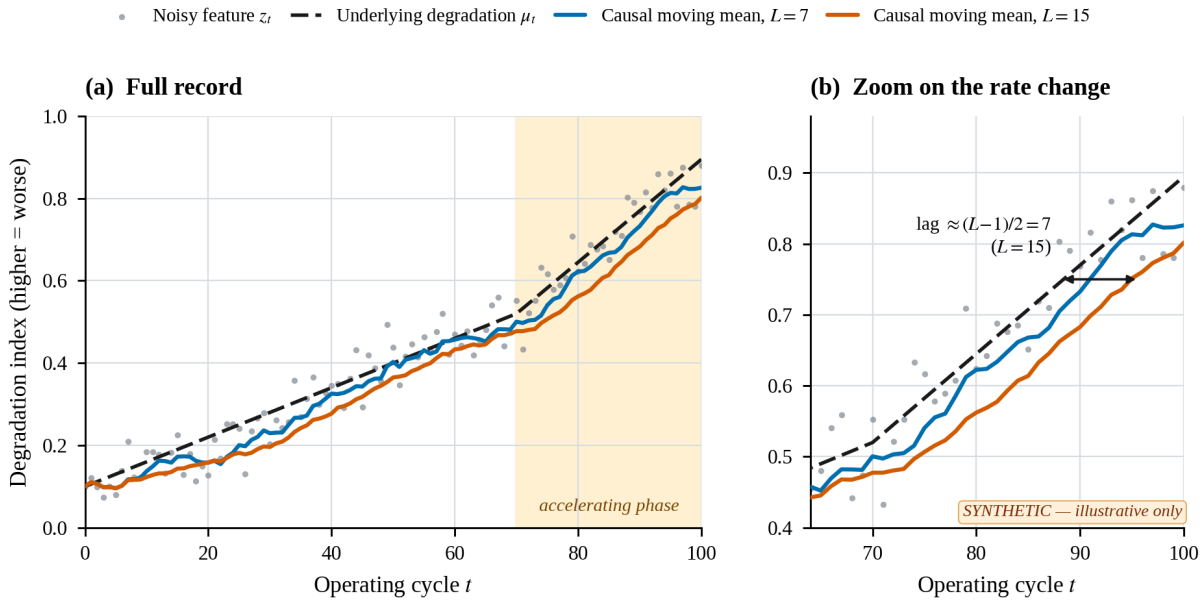


Figure 2. Illustrative degradation signal showing the trade-off between noise reduction and responsiveness

Figure 2 illustrates the trade-off that motivates this study. Panel (a) shows a noisy degradation index over 100 cycles that rises more steeply in an accelerating phase after about cycle 70, together with causal moving means of length 7 and 15. Panel (b) zooms on the rate change and shows that the moving means lag the underlying state by about $(L - 1)/2$ samples, seven samples for $L = 15$. All values are synthetic, and the figure shows that the longer window removes more noise at the cost of more delay.

3. Methodology

3.1 Signal, Feature and Degradation State

Let *x*t be the vector of sensor readings at operating index *t*, such as RMS vibration, kurtosis, bearing temperature, motor current or oil-debris count. The feature map, the causal summability operator and its weight conditions are given in Equations 1 to 3.

$$z_t = \phi\left(x_{t-w+1}, \ldots, x_t\right) \tag{1}$$

$$s_t = \sum_{j=0}^{L-1} a_j z_{t-j} \tag{2}$$

$$a_j \geq 0, \sum_{j=0}^{L-1} a_j = 1 \tag{3}$$

Equation 1 maps a recent window of w raw readings to a health-related feature zt, with standardization constants estimated from training data only and the indicator oriented so that a larger value means a worse condition. Equation 2 defines the smoothed value st as a weighted sum of the latest L features, with weights indexed by lag j so that $j = 0$ is the newest observation. Equation 3 requires the weights to be nonnegative and to sum to one. These conditions keep a constant input unchanged and keep st within the range of the averaged values, which avoids artificial overshoot but does not make the output monotonic when the input is noisy.

3.2 Finite-Window, Cesàro-Type and Exponential Means

The specific operators used in the framework are given in Equations 4 to 7.

$$s_t = \frac{1}{L} \sum_{j=0}^{L-1} z_{t-j} \tag{4}$$

$$s_t = \frac{1}{t} \sum_{i=1}^{t} z_i \tag{5}$$

$$s_t = \alpha z_t + (1-\alpha) s_{t-1}, 0 < \alpha \leq 1 \tag{6}$$

$$h_{1/2} = \frac{ln\left(0.5\right)}{ln\left(1-\alpha\right)}, 0 < \alpha < 1 \tag{7}$$

Equation 4 is the L-point moving mean, which sets every weight to $1/L$ and is simple and cheap to compute. Equation 5 is the cumulative mean, which is closely related to Cesàro averaging but becomes increasingly sluggish because early observations keep their influence, so at start-up the weights should be renormalized over the available observations rather than padded with zeros. Equation 6 is the exponentially weighted mean, whose lag weights are proportional to $\alpha(1 - \alpha)$j, so a large α follows changes quickly while a small α removes more noise. Equation 7 gives the half-life of the filter memory in samples, which lets engineers state the memory in cycles or operating hours. Table 2 summarizes these and two further operators.

Table 2. Summability operators used in the proposed framework

Operator	Weights / recurrence	Advantages	Risk to monitor
Uniform finite mean	$a_j=1/L$	Easy to explain and audit	Window-induced delay
Cumulative arithmetic mean	$s_t=(1/t)\Sigma z_i$	Stable long-run average	Adapts slowly after regime change
Exponential mean	$s_t=\alpha z_t+(1-\alpha)s_{t-1}$	Efficient, recency-aware	Parameter sensitivity
Triangular weighted mean	$a_j \propto L-j$	Recent samples receive greater weight	Choice of kernel may be arbitrary
Robust mean / median hybrid	Trim or winsorize, then average	Reduces isolated spikes	May suppress real impulsive fault cues

Table 2 compares five operators by their weights, advantages and the risk to monitor. The uniform finite mean is easy to explain but introduces window-induced delay, and the cumulative mean gives a stable long-run average that adapts slowly after a regime change. The exponential mean is efficient and recency-aware but sensitive to its parameter, and the triangular mean gives recent samples more weight through a kernel that may be arbitrary. The robust median hybrid reduces isolated spikes but may suppress genuine impulsive fault cues.

3.3 Noise and Stability

Suppose zt = μt + εt, where μt is the underlying degradation level and εt is zero-mean noise. The variance and bias of the smoothed value are given in Equations 8 to 11.

$$Var\,(s_t) = \sigma^2 \sum_j a_j^2 \tag{8}$$

$$Var\,(s_t) = \sum_i \sum_j a_i a_j \gamma\,(i-j) \tag{9}$$

$$b_t = E\,[s_t] - \mu_t = \sum_j a_j \mu_{t-j} - \mu_t \tag{10}$$

$$b_t = -\beta_1 \sum_j j a_j \tag{11}$$

Equation 8 gives the variance under independent noise with variance σ2, which equals σ2/L for a uniform L-point mean. Equation 9 generalizes it to correlated noise with autocovariance $\gamma(k)$, showing that the familiar reduction to σ2/L is optimistic when neighbouring sensor values are correlated. Equation 10 defines the smoothing bias as the gap between the expected smoothed value and the current level. Equation 11 shows that for a locally linear trend μt = β0 + β1t the bias equals the slope times the weighted mean lag, so noise reduction must always be traded against detection delay.

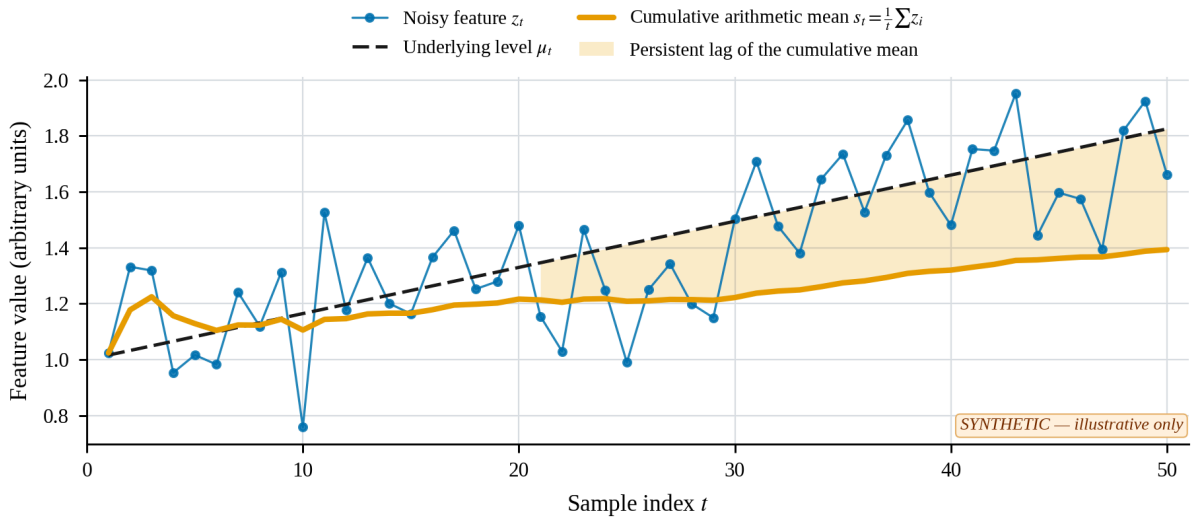


Figure 3. Cumulative arithmetic averaging of a noisy feature stream and its persistent lag

Figure 3 illustrates this lag with a cumulative arithmetic mean over 50 samples. The noisy feature scatters between about 0.8 and 1.9 around an underlying level that rises steadily from 1.0 to about 1.8. The cumulative mean flattens the noise but rises only to about 1.4 by the last sample. The shaded gap between the mean and the underlying level is the persistent lag predicted by Equation 11, and the series is synthetic.

3.4 RUL Mapping and Uncertainty

Let st be the smoothed degradation index and θ the pre-specified end-of-useful-life threshold. The local slope and the threshold-crossing estimate are given in Equations 12 and 13.

$$\hat{\beta}_t = \frac{\sum_i \left(t_i - \bar{t}\right)\left(s_i - \bar{s}\right)}{\sum_i \left(t_i - \bar{t}\right)^2} \tag{12}$$

$$\hat{R}_t = max\left\{0, \frac{\theta - s_t}{\hat{\beta}_t}\right\} \tag{13}$$

Equation 12 estimates the recent degradation slope by ordinary least squares over the latest m smoothed values. Equation 13 divides the remaining distance to the threshold by this slope and truncates the result at zero. If the estimated slope is not positive, the formula gives no finite positive forecast, so the system should report an indeterminate estimate rather than divide by a very small number. The linear model is intentionally transparent rather than universally adequate, because fatigue, corrosion, wear and ageing may be nonlinear and maintenance may reset the state, so exponential, stochastic-process, state-space or learned models may be preferable (Li, Wei, He, Yang, & Meng, 2023; Si, Wang, Hu, & Zhou, 2011).

A credible system should report an inter14val rather than only a point estimate, for example by bootstrapping complete run-to-failure units, using Bayesian state-space models or quantile regression, and calibrating intervals on held-out units (Zhan, Kong, Wang, Jin, & Xu, 2024; Zhu, Chen, Peng, & Ye, 2022). When the threshold, the current index and the slope are all uncertain, the delta method gives the approximate variance in Equation 14.

$$Var\,(R) \approx \left(\frac{\partial R}{\partial \theta}\right)^2 \sigma_\theta^2 + \left(\frac{\partial R}{\partial s}\right)^2 \sigma_s^2 + \left(\frac{\partial R}{\partial \beta}\right)^2 \sigma_\beta^2 \tag{14}$$

In Equation 14, the partial derivatives are $\partial R/\partial\theta = 1/\beta$, $\partial R/\partial s = -1/\beta$ and $\partial R/\partial\beta = -(\theta - s)/\beta 2$, and covariances are ignored. The approximation becomes unstable when β is near zero, because the last derivative grows rapidly. Simulation is often safer, sampling plausible values of θ, s and β, rejecting invalid combinations by predeclared rules and reporting quantiles. The report should also state whether the uncertainty reflects measurement noise, parameter uncertainty, operating-regime uncertainty or all three (Betz, Papaioannou, & Straub, 2022; Kala, 2022).

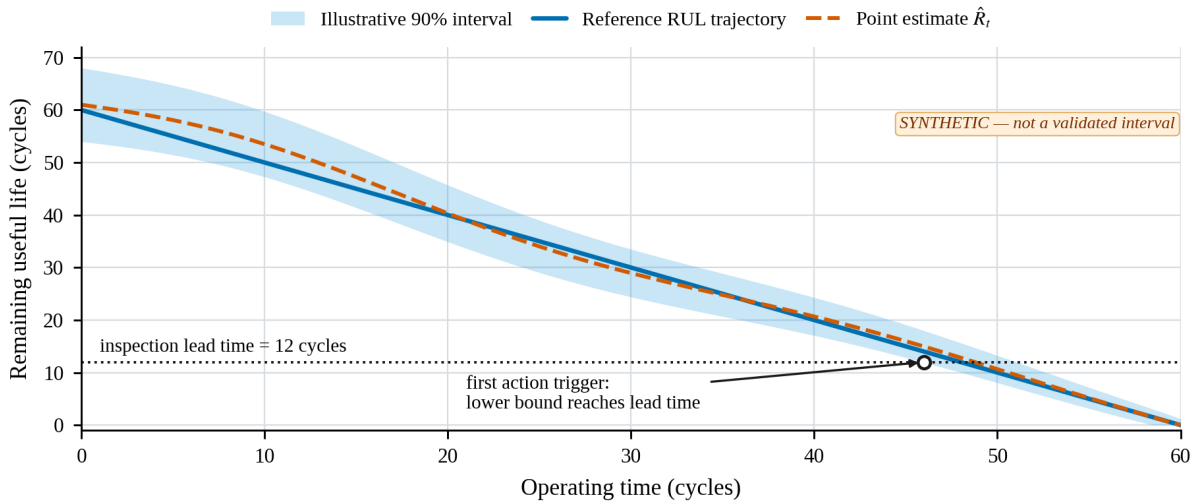


Figure 4. Point RUL trajectory with an illustrative uncertainty band and first action trigger

Figure 4 shows a point RUL trajectory with an illustrative 90% band over 60 operating cycles. The point estimate stays close to the reference trajectory as both decline from about 60 cycles to zero. A dotted line marks an inspection lead time of 12 cycles, and the first action is triggered at about cycle 46, when the lower bound reaches this lead time. The values are synthetic and are not a validated prediction interval. Maintenance decisions depend on both RUL and consequences. A conservative policy may schedule inspection when the lower bound approaches a lead-time threshold, while a low-consequence component may tolerate a higher chance of run-to-failure, and a rule can compare expected costs of planned maintenance, failure and inspection. The preferred action is not necessarily the one with the smallest point error, because downtime, spare parts, safety and production schedules all matter (Ait, Laggoune, & Chateauneuf, 2023; Liu, & Wang, 2022).

3.5 Processing Pipeline and Algorithm

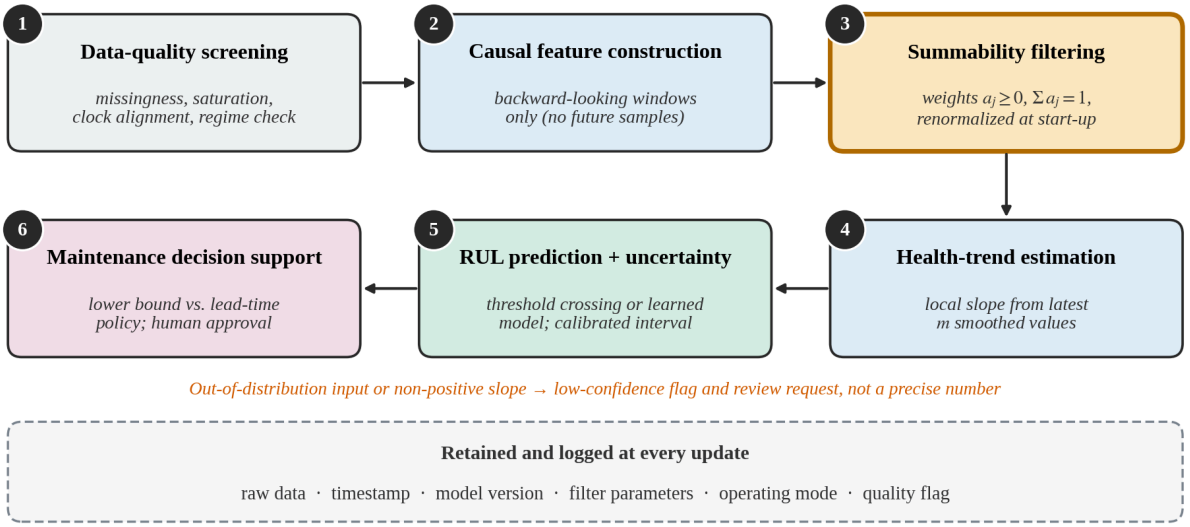


Figure 5. End-to-end causal processing pipeline with quality checks and model governance

Figure 5 shows the six processing stages. Data-quality screening checks missingness, saturation, clock alignment and regime, and causal feature construction uses only backward-looking windows. Summability filtering applies normalized weights that are renormalized at start-up, health-trend estimation computes a local slope, and RUL prediction adds a calibrated interval before maintenance decision support compares the lower bound with the lead-time policy under human approval. Out-of-distribution inputs or non-positive slopes produce a low-confidence flag, and raw data, timestamps, model version, filter parameters, operating mode and quality flags are logged at every update.

At each update, the algorithm validates timestamps, sensor ranges, missingness and operating regime, then computes the feature from current and preceding samples only and applies Equation 2 with available, renormalized weights. It estimates the degradation rate from the latest smoothed values, computes the threshold-crossing RUL if the rate is valid and flags the estimate as indeterminate otherwise. An interval is then estimated by a calibrated probabilistic model or a unit-level bootstrap, policy thresholds are applied to the lower bound, uncertainty and consequence class, and raw features, smoothed features, estimate, interval, flags and model version are logged. The output is an RUL estimate, an interval, an action suggestion and an auditable diagnostic record.

Kernel selection should take place insid15e training and validation, using nested unit-wise splits, rather than by inspecting the test trajectory. The selection objective can combine accuracy, late alarms and calibration, as in Equation 15.

$$J = \lambda_1 \mathrm{MAE} + \lambda_2 \mathrm{LateAlarmRate} + \lambda_3 \left|\mathrm{Coverage} - (1-q)\right| \tag{15}$$

Equation 15 weights the mean absolute error, the late-alarm rate and the gap between empirical coverage and the nominal level $1 - q$. The weights $\lambda 1$, $\lambda 2$ and $\lambda 3$ are policy choices that must be declared before test evaluation. A filter with the lowest error may still be unacceptable if it systematically delays warnings. The objective therefore makes the trade-off between accuracy and timeliness explicit.

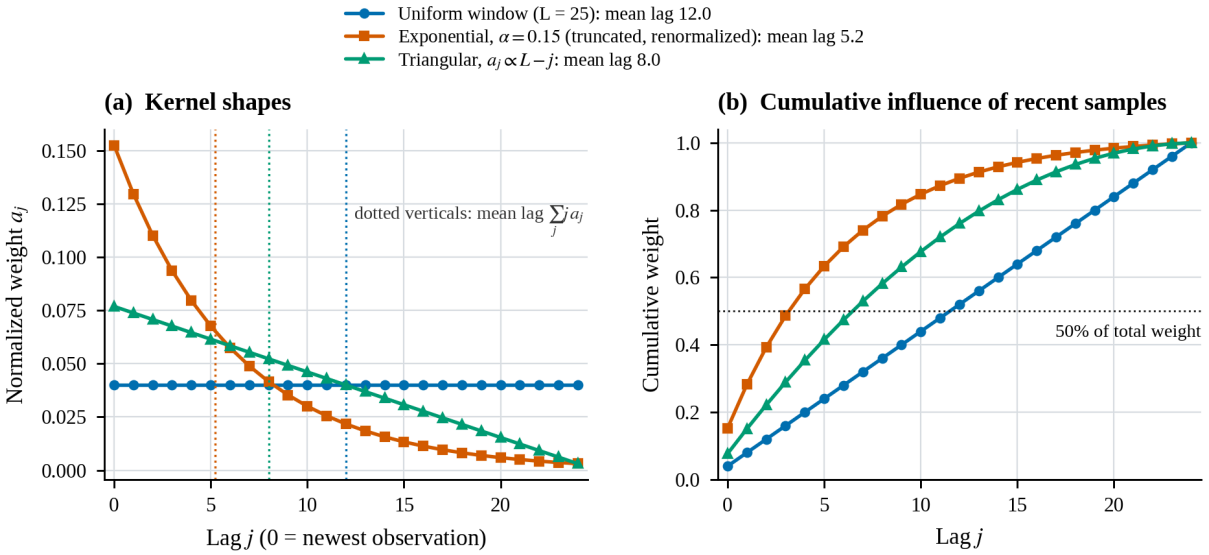


Figure 6. Example normalized weighting kernels by lag and cumulative weight

Figure 6 compares three normalized kernels over 25 lags. Panel (a) shows that a uniform window of 25 has a mean lag of 12.0, a triangular kernel 8.0, and an exponential kernel with $\alpha = 0.15$ only 5.2. Panel (b) shows cumulative weight, where the exponential kernel reaches half its weight within about four lags while the uniform kernel needs about 12. The kernel shape therefore determines responsiveness as much as the window length.

3.6 Evaluation Metrics and Validation Protocol

For N test predictions with predicted RUL and true RUL, the accuracy and interval metrics are given in Equations 16 and 17.

$$\mathrm{MAE} = \frac{1}{N}\sum_{i=1}^{N}\left|\hat{R}_i - R_i\right|, \quad \mathrm{RMSE} = \sqrt{\frac{1}{N}\sum_{i=1}^{N}\left(\hat{R}_i - R_i\right)^2} \tag{16}$$

$$Coverage = \frac{1}{N}\sum_{i=1}^{N} 1\left(L_i \le R_i \le U_i\right), Width = \frac{1}{N}\sum_{i=1}^{N}\left(U_i - L_i\right) \tag{17}$$

Equation 16 gives the mean absolute error and root mean squared error, the first easier to interpret in the target unit and the second more sensitive to large errors. Equation 17 gives interval coverage, the share of true values inside the predicted interval, and mean interval width. Coverage should always be reported with width, because an extremely wide interval can reach nominal coverage while being useless for maintenance. Warning lead time, the time between the first valid alarm and the end point, should be reported alongside these metrics (Zhan et al., 2024).

A credible study should compare at least three baselines, namely raw features with the same RUL model, a simple moving mean and exponential smoothing, with the same features, targets, splits and downstream predictor for all methods. Data must be split by asset or run-to-failure unit, never randomly by overlapping windows, and filter parameters must be tuned on validation units only, with bootstrap confidence intervals at the asset level. The recommended metrics are summarized in Table 3.

Table 3. Recommended evaluation metrics and interpretation

Metric	Definition / unit	What it reveals	Caution
MAE	Mean absolute RUL error	Typical absolute error	Does not show tail risk
RMSE	Root mean squared error	Sensitivity to large misses	Can be dominated by outliers
Interval coverage	Fraction within interval	Calibration	Pair with interval width
Interval width	Mean upper−lower bound	Precision of uncertainty	Narrow is not automatically better
Warning lead time	Hours/cycles before end point	Operational usefulness	Must specify alarm rule
False-alarm rate	Events per asset-time	Maintenance burden	Requires exposure denominator
Late-alarm rate	Fraction warning too late	Safety / availability risk	Define required lead time

Table 3 defines each metric with its unit, what it reveals and a caution. The mean absolute and root mean squared errors summarize accuracy but hide timing, while coverage and width describe interval quality only when read together. Lead time and the false and late alarm rates connect predictions to maintenance consequences. The table shows that no single number can judge an RUL method.

Table 4. Candidate hyperparameters for a controlled experiment

Parameter	Candidate values	Selection rule	Leakage control
Moving window L	3, 5, 9, 15 samples	Validation objective	Choose using validation units only
Exponential α	0.15, 0.30, 0.50, 0.70	Joint accuracy and lead-time score	Freeze before test
Slope history m	5, 10, 20 samples	Stability of local fit	Use causal history
Threshold θ	Engineering-defined per feature	OEM / inspection / policy basis	Do not tune on test failures
Interval level	80%, 90%, 95%	Calibration on validation units	Report held-out coverage
Alarm lead time	Asset-specific policy	Reliability and safety review	Pre-register policy

Table 4 lists the candidate hyperparameters for a controlled experiment. Each parameter is given its candidate values, a selection rule and a leakage control. Window lengths and α values are chosen by rolling or nested validation on training units only. The leakage controls ensure that the final test units play no part in choosing the filter.

Table 5. Minimum data and governance requirements

Item	Minimum specification	Reason
Asset identity	Stable ID and equipment family	Prevents train/test confusion
Timestamp	Timezone, sampling interval, gap flags	Preserves chronological order

Item	Minimum specification	Reason
Sensor metadata	Units, calibration, location, range	Supports comparable features
Maintenance events	Inspection, repair, replacement, overhaul	Separates degradation from resets
Failure definition	Threshold, event type, censoring rule	Makes target reproducible
Operating context	Load, speed, ambient conditions	Controls regime confounding
Data split	Asset-wise and chronological	Limits leakage
Versioning	Feature code, filter, model, policy	Enables audit and rollback

Table 5 sets out the minimum data and governance requirements. It covers stable asset identity, synchronized timestamps, units, maintenance-event codes, a consistent failure definition and model versioning, each with the reason it is needed. Without these, even a sophisticated RUL model learns inconsistent labels. The table also serves as a checklist before any pilot deployment, in the same way that numerical tools elsewhere are checked against field measurements before use (Putra et al., 2023).

4. Results and Discussion

4.1 Analytical Findings

Several results follow mathematically from Section 3. For independent equal-variance noise, a normalized weighted mean reduces variance by the factor Σ*aj*2, recency weighting reduces lag under a rising trend, the same change usually raises variance because fewer samples are effectively averaged, and threshold-crossing RUL is highly sensitive to slope error when the slope is small. The effective sample size in Equation 18 summarizes the variance reduction.

$$n_{eff} = \frac{1}{\sum_j a_j^2} \tag{18}$$

Equation 18 defines the effective sample size as the reciprocal of the sum of squared weights. A uniform L-point mean has $n$eff = L, while an exponential filter with an infinite tail has Σ*aj*2 = α/(2 − α) and therefore $n$eff = (2 − α)/α, which is about 5.7 for α = 0.3. The exponential filter thus averages fewer samples than a long window but responds faster to change. Under autocorrelation, $n$eff overstates the independent information and should be treated as a diagnostic. Table 6 compares the two main operators under idealized assumptions.

Table 6. Analytical comparison under idealized assumptions

Property	Uniform finite mean	Exponential mean	Implication for RUL
Constant preservation	Yes, normalized weights	Yes, normalized weights	No artificial level shift for constant input
Independent-noise variance	σ^2/L	$\sigma^2\Sigma a_j^2$	Longer memory reduces variance
Trend lag	Mean lag (L−1)/2	(1−α)/α for infinite tail	More recency weighting reduces lag

Property	Uniform finite mean	Exponential mean	Implication for RUL
Step-change response	Gradual over L samples	Geometric approach	Window/α must match warning needs
Compute cost per update	O(L), or O(1) running sum	O(1)	Both are feasible at edge
Interpretability	High	High	Supports maintenance auditability

Table 6 compares the uniform and exponential means on six properties. Both preserve constants because their weights are normalized, and their independent-noise variances are $\sigma 2/L$ and $\sigma 2\Sigma aj2$. The mean lag is $(L - 1)/2$ for the uniform mean and $(1 - \alpha)/\alpha$ for the exponential mean, so more recency weighting reduces lag. Both cost little per update and remain highly interpretable, which supports maintenance auditability.

4.2 Worked Example: Motor-Driven Pump

Consider a centrifugal pump supplying process water in a small manufacturing plant, with a motor-mounted accelerometer recording vibration features every operating hour and bearing temperature and motor current as corroborating signals. The threshold is set from engineering limits, manufacturer guidance, inspection evidence and plant policy rather than from the model. Five recent normalized feature values are 0.62, 0.67, 0.64, 0.73 and 0.76, where higher means worse. Table 7 shows how the two filters respond.

Table 7. Worked pump example: recent normalized health features

Hour index	Raw feature z_t	5-point mean*	Exponential mean (α=0.5)*	Interpretation
t−4	0.62	0.620	0.620	Baseline within this short window
t−3	0.67	0.645	0.645	Increase may reflect wear or load
t−2	0.64	0.643	0.643	Small reversal; not necessarily recovery
t−1	0.73	0.665	0.686	Rise becomes more persistent
t	0.76	0.684	0.723	Recent rise remains visible

Table 7 lists the raw feature, the running five-point mean and the exponential mean with $\alpha = 0.5$ for each hour. The five-point mean at the last hour is $(0.62 + 0.67 + 0.64 + 0.73 + 0.76)/5 = 0.684$, which damps the latest rise to 0.76. The exponential mean, initialized at 0.62, gives 0.645, 0.643, 0.686 and 0.723, and therefore reacts faster because it weights recent readings more. The interpretation column notes that the small reversal at hour $t - 2$ is not necessarily recovery and that the recent rise remains visible.

Assume, solely for demonstration, a thre19shold of 1.00, a smoothed index of 0.723 and a slope of 0.0045 index units per hour from a longer illustrative sequence. Equation 19 gives the resulting estimate.

$$\hat{R}_t = \frac{1.00 - 0.723}{0.0045} \approx 61.6 hours \tag{19}$$

Equation 19 applies Equation 13 and gives about 61.6 hours. The number is only as credible as its assumptions of a stable local rate, a correct threshold, comparable future duty and a meaningful health index. If a calibrated model produced a lower 10th-percentile estimate of 34 hours and inspection needs 12 hours of lead time, the lower bound would leave a 22-hour buffer. The 34-hour value is a hypothetical illustration of how a lower bound is used, not an interval computed from the five data points.

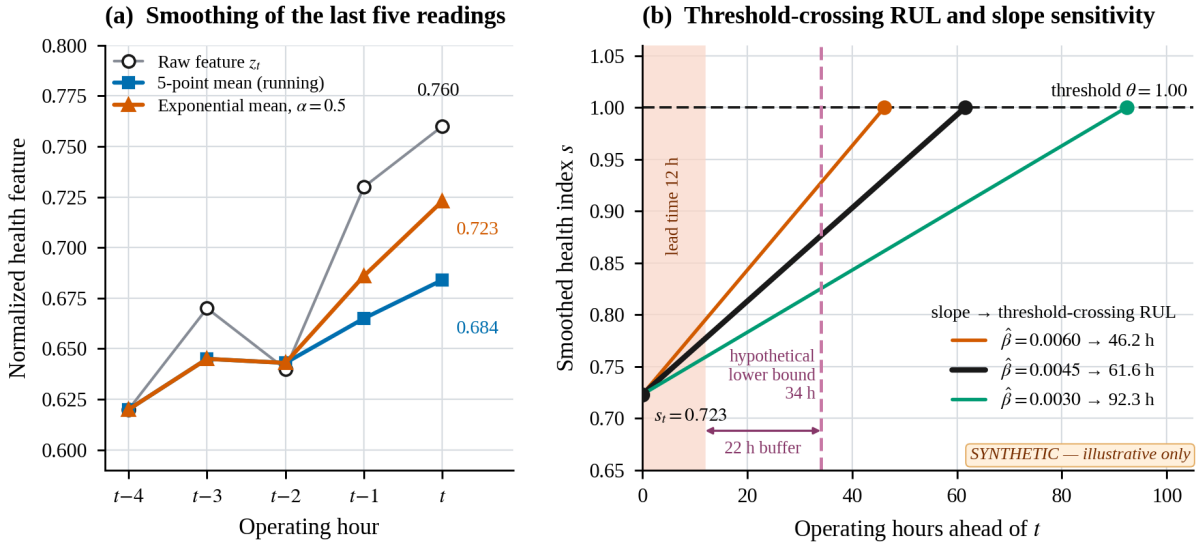


Figure 7. Worked pump example: smoothing and threshold-crossing RUL sensitivity

Figure 7 plots the example. Panel (a) shows the raw feature rising to 0.760 while the five-point mean reaches 0.684 and the exponential mean 0.723. Panel (b) shows threshold-crossing RUL for three slopes, 46.2 hours at 0.0060, 61.6 hours at 0.0045 and 92.3 hours at 0.0030, with the 12-hour lead time and the hypothetical 34-hour lower bound marked. The spread shows how strongly RUL depends on the slope estimate.

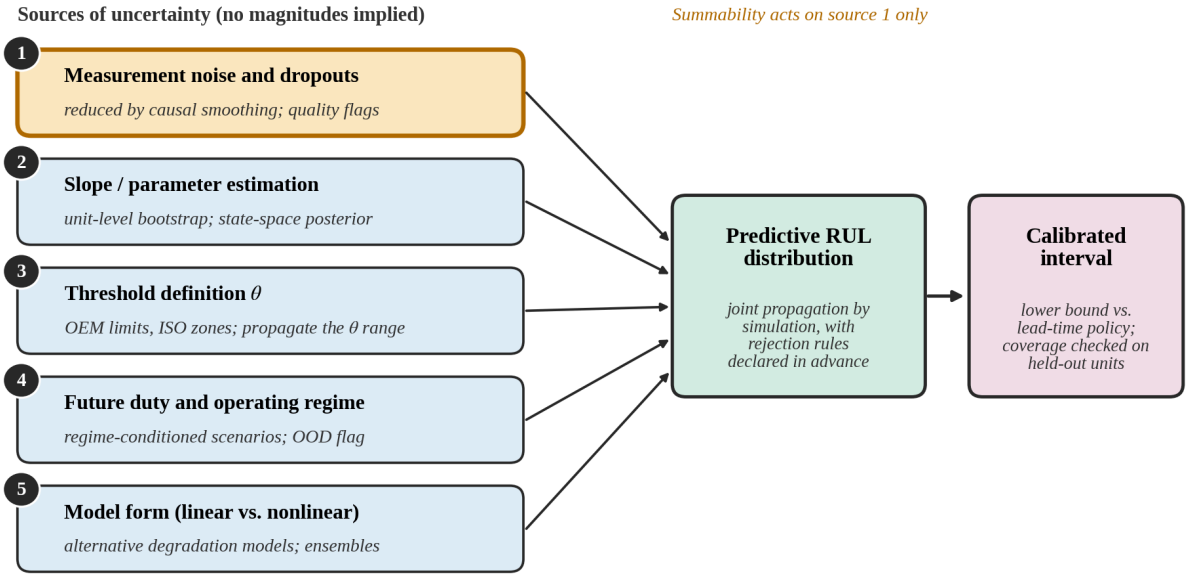


Figure 8. Conceptual sources of uncertainty in RUL estimation and the stage that addresses each

The appropriate action is to verify the signal before escalating maintenance, by checking sensor mounting and calibration, recent valve or load changes, temperature and current, and the vibration spectrum for bearing frequencies. Figure 8 maps five sources of uncertainty to the stage that addresses each. Measurement noise and dropouts are reduced by causal smoothing and quality flags, slope estimation by unit-level bootstrap or state-space posteriors, threshold definition by propagating the range of θ, future duty by regime-conditioned scenarios, and model form by alternative models or ensembles. These feed a predictive RUL distribution and a calibrated interval, and summability acts on the first source only.

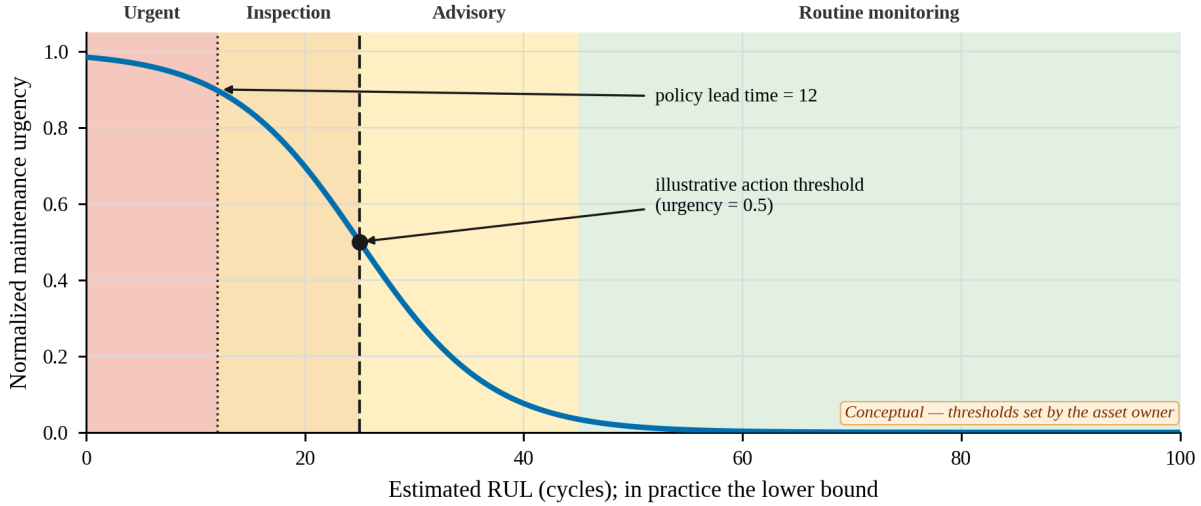


Figure 9. Illustrative maintenance urgency curve against estimated RUL

Figure 9 shows a conceptual maintenance urgency curve against estimated RUL. Urgency stays near zero for RUL above about 60 cycles in a routine-monitoring zone and rises through advisory and inspection zones as RUL falls. The policy lead time is marked at 12 cycles and an illustrative action threshold at an urgency of 0.5, near 25 cycles. In practice the curve should be applied to the lower bound, and the thresholds must be set by the asset owner.

4.3 Sensitivity of the Pump Estimate

A slope of 0.0060 would shorten the RUL to about 46.2 hours, and a slope of 0.0030 would lengthen it to about 92.3 hours, so a modest slope error moves the maintenance date substantially. The sensitivities to slope, threshold and filter length are given in Equations 20 to 22.

$$\frac{\partial R}{\partial \beta} = -\frac{\theta - s}{\beta^2} \tag{20}$$

$$\frac{\partial R}{\partial \theta} = \frac{1}{\beta} \tag{21}$$

$$-\beta \frac{L-1}{2} \tag{22}$$

Equation 20 shows that the sensitivity of RUL to the slope is $-(\theta - s)/\beta 2$, whose magnitude grows as the slope approaches zero, so a model should report low confidence when the slope is small. Equation 21 shows that for fixed s and β the sensitivity to the threshold is $1/\beta$, so uncertainty in the acceptable limit passes directly into RUL. Equation 22 gives the bias of a uniform window of length

L under a linear trend, $-\beta(L-1)/2$, so the mean lag is 4 samples for $L = 9$ and 7 samples for $L = 15$. If one sample is one hour and the slope is 0.0045 per hour, the 15-sample window understates the current index by about 0.032, which shifts the RUL estimate by several hours.

4.4 Real-Life Application Classes and the IMS Bearing Record

Table 8. Real-life application classes, public data sources and the role of the summability stage

Asset class	Condition data	Health indicator and end point	Role of the summability stage	Main caution
Aircraft turbofan engines	NASA C-MAPSS: multivariate sensor sequences, several operating conditions and fault modes (simulated) (Saxena et al., 2008)	Fused sensor features; simulated end of life	Smooth noisy channels before trend or learned RUL estimation	Simulated data, not field records
Rolling-element bearings in motors, pumps and gearboxes	NASA/IMS bearing run-to-failure tests (Qiu et al., 2006); PRONOSTIA (PHM 2012) vibration and temperature (Nectoux et al., 2012)	Vibration features such as RMS; end point from failure or a vibration limit	Stabilize slowly rising features; keep envelope features unsmoothed in parallel	Laboratory rigs; long windows can delay abrupt onset
Lithium-ion batteries	NASA cell cycling data (Goebel et al., 2008)	Capacity fade; end of life at a capacity threshold	Reduce measurement noise on capacity	Capacity can partially recover after rest; smoothing must not hide it
Motor-driven centrifugal pumps in a plant	Plant vibration, temperature, current and maintenance logs; vibration evaluation per ISO 20816 (ISO, 2022)	Vibration-derived health index; threshold from OEM limits and standards	Suppress valve and load transients; causal exponential mean on an edge gateway	No public benchmark; needs plant labels and censoring rules (Zio, 2022)

Table 8 maps four asset classes to their condition data, health indicator and end point, the role of summability and the main caution. Aircraft turbofans use the simulated C-MAPSS data, rolling-element bearings use the NASA/IMS and PRONOSTIA run-to-failure records, lithium-ion batteries use NASA cycling data, and plant pumps rely on vibration, temperature, current and maintenance logs evaluated against ISO 20816. In each case summability stabilizes slowly rising features, while envelope features or capacity recovery must not be smoothed away. The pump class has no public benchmark and needs plant labels and censoring rules.

A hypothetical deployment at a municipal water-supply pumping station illustrates the route. For a duty and standby pair of pumps rated above 15 kW, within the scope of ISO 20816-3 (ISO, 2022), hourly RMS vibration velocity, bearing temperature and motor current would be normalized with baseline statistics, the threshold would come from the manufacturer limit and the standard, and an exponential mean with $\alpha = 0.3$ would be applied, with a half-life of about 1.9 hours and a mean lag

of about 2.3 hours. The system would run in shadow mode for at least one maintenance cycle before the lower bound of the RUL interval, compared with a 12-hour lead time, is used to raise work orders, as with other digital maintenance tools introduced in power generation (Imantha et al., 2026).

The strongest public case is the NASA/IMS bearing experiment, which recorded the natural wear-out of a bearing rather than a seeded defect (Qiu et al., 2006). Four double-row bearings ran on one shaft at 2,000 r/min under a 6,000 lb radial load until an outer-race defect developed on Bearing 1 in Test 2, and a 1-second vibration snapshot was stored every 10 minutes, giving 984 snapshots or about 164 hours. Table 9 lists the documented facts and the settings used here.

Table 9. Real-life application on NASA/IMS Test 2, Bearing 1: documented data and framework settings

Item	IMS Test 2 (documented)	Setting in this framework
Rig and load	Four Rexnord ZA-2115 double-row bearings on one shaft; 2000 r/min; 6000 lb radial load; force-lubricated (Qiu et al., 2006)	Bearing 1 only; constant duty, so no regime shift is expected
Recording	20 480 samples (1 s at 20.48 kHz) every 10 min; 984 snapshots, about 164 h	One snapshot = one sample of the sequence; 1 s per 600 s = 0.17% duty cycle
Failure	Natural outer-race defect on Bearing 1 (not seeded); outer-race fault frequency about 236 Hz	End point defined by a vibration threshold, not by teardown time alone
Health index	One accelerometer channel per bearing	RMS per snapshot, divided by the mean of the first 100 snapshots (baseline only)
Summability stage	Not applicable in the source data	Causal exponential mean, α=0.30: half-life 1.9 snapshots (19 min), mean lag 2.3 snapshots (23 min)
Rate and RUL	Not provided	OLS slope over 60 snapshots (10 h); RUL=$(\theta - s_t)/\beta_t$; indeterminate if slope is not positive
Thresholds	Not provided	θ=4× baseline and first-alarm level 2× baseline: illustrative policy values, to be fixed before testing
Reporting	n/a	False first alarm, lead time, interval coverage; raw feature and moving mean as baselines (Section 3.8)

Table 9 pairs each documented item with the corresponding framework setting. The health index is RMS per snapshot divided by the mean of the first 100 snapshots, and the summability stage is a causal exponential mean with $\alpha = 0.30$, giving a half-life of 1.9 snapshots (19 minutes) and a mean lag of 2.3 snapshots (23 minutes). The slope is estimated over 60 snapshots (10 hours), the threshold is four times baseline and the first-alarm level twice baseline, both fixed before testing. The record suits summability because each snapshot samples only 1 second in 600, the degradation is slow and accelerating, and the filter lag is negligible against a 12-hour lead time.

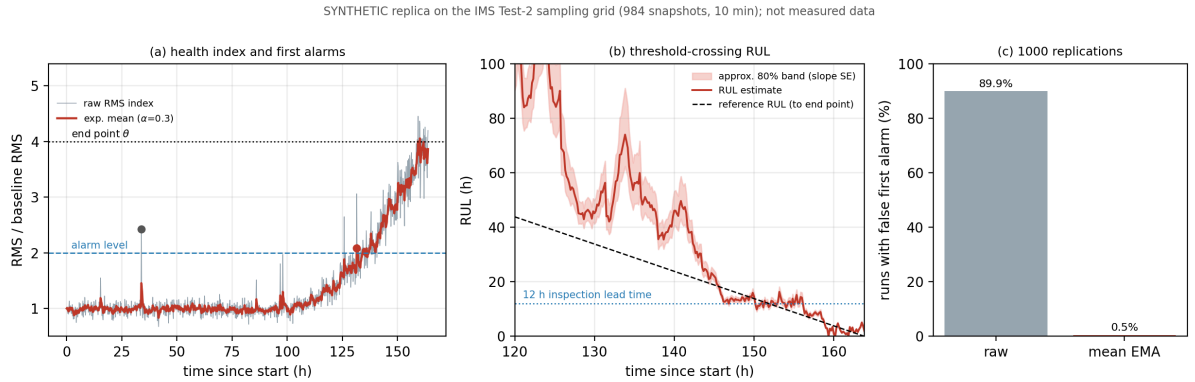


Figure 10. Application on the IMS Test 2 configuration using a synthetic replica

Figure 10 shows the pipeline on a synthetic replica of the IMS Test 2 sampling grid, because the raw files cannot be redistributed. Panel (a) shows the raw and smoothed RMS index with the first alarm of each rule, panel (b) the threshold-crossing RUL with an approximate slope-based band and the 12-hour lead time, and panel (c) the share of 1,000 replications whose first alarm is false, 89.9% for the raw index against 0.5% for the exponential mean. Among valid alarms, the median lead time was 34.7 hours for the raw index and 30.3 hours for the exponential mean, against an ideal 29.2 hours, and the RUL band does not cover the reference during early acceleration, so it is not a calibrated interval. These outcomes follow from the simulation and are not claims about the real bearing, which the accompanying script can process with the measured files.

4.5 Monte Carlo and Ablation Demonstrations

A Monte Carlo experiment isolates transient-induced false alarms versus detection delay. A latent feature stays at 0.30 until hour 250 and then rises to 1.00 at hour 400, with Gaussian noise (σ = 0.06) and short transients that mimic valve transitions. An alarm is raised when the processed feature first reaches 0.60 and counted as false if the latent feature is below 0.45, and an ideal alarm gives a 64-hour lead time. These settings follow change-point and EWMA monitoring designs (M. Li et al., 2025; Xie et al., 2022).

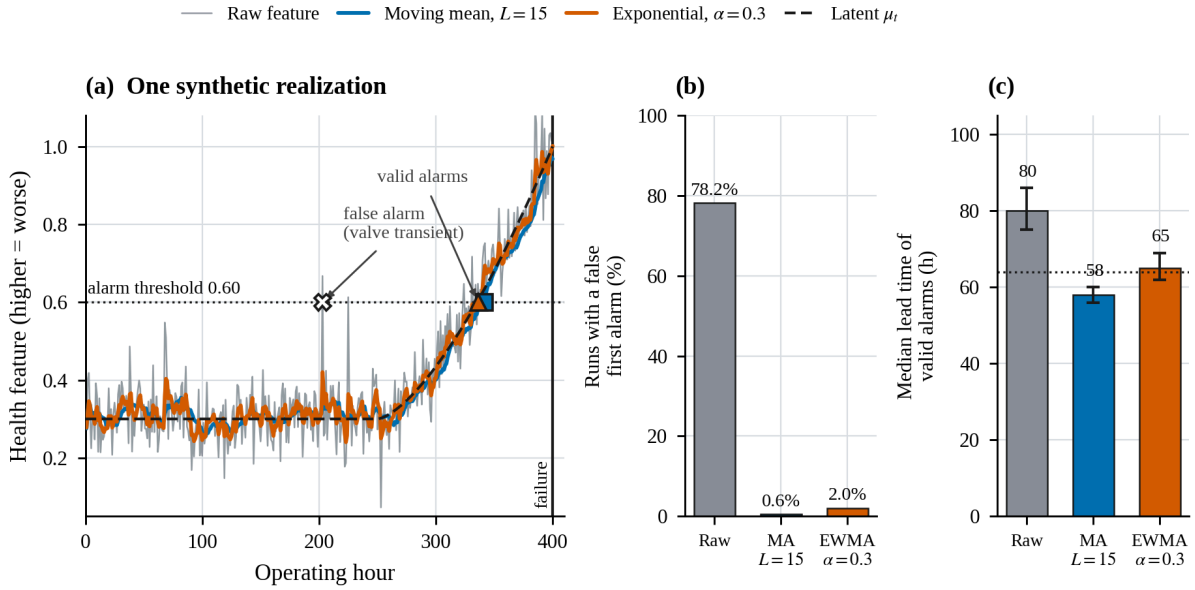


Figure 11. Monte Carlo comparison of alarm rules on 2,000 synthetic pump runs

Figure 11 reports the results over 2,000 runs. Panel (a) shows one realization with a false alarm caused by a valve transient. Panel (b) shows that the first alarm of the raw feature was false in 78.2% of runs, against 0.6% for the 15-point moving mean and 2.0% for the exponential mean with α = 0.3. Panel (c) gives median lead times of valid alarms of 80 hours for the raw feature, 58 for the

moving mean and 65 for the exponential mean, where the raw value reflects noise-driven early crossings and the moving mean gives up about 6 hours to its 7-hour lag.

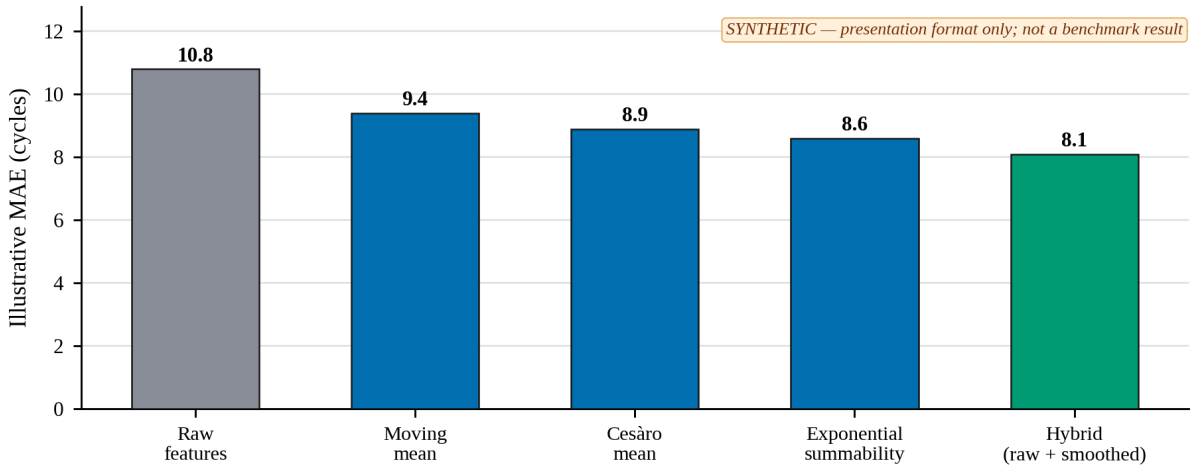


Figure 12. Synthetic ablation chart demonstrating presentation format only

Figure 12 demonstrates how an ablation chart should be presented, using deliberately invented mean absolute errors. The bars fall from 10.8 cycles for raw features to 9.4 for the moving mean, 8.9 for the Cesàro mean, 8.6 for exponential summability and 8.1 for a raw-plus-smoothed hybrid. These values are not measured on C-MAPSS, a pump or any benchmark and must not be cited as evidence. A real comparison must publish the data partition, seeds, preprocessing, RUL cap, scoring code, confidence intervals and per-regime results.

4.6 Discussion

Summability-based preprocessing is most attractive when the prognostic signal changes more slowly than short-term noise and when the noise is not dominated by meaningful impulsive events. It offers low computational cost, clear mathematical behavior and an audit trail that maintenance staff can follow, and its modularity lets the same smoother feed a trend model, a random forest, a recurrent network or a state-space estimator (Bai et al., 2023; Nguyen et al., 2022). Smoothing is dangerous when fault onset is abrupt, when high-frequency transients are diagnostic or when the feature is already clean, and averaging may blend operating regimes, so event-sensitive features such as envelope spectra should bypass low-pass filtering (Guo, Li, & Wan, 2023). A single scalar health index can also hide competing failure modes such as bearing wear, impeller damage, cavitation and misalignment, so each feature should receive domain-aware parameters. Table 10 compares the main preprocessing strategies.

Table 10. Practical trade-offs across preprocessing strategies

Strategy	Noise suppression	Transient sensitivity	Interpretability	Deployment burden
No smoothing	Low	Highest	High	Very low
Moving mean	Moderate-high	Lower for long windows	High	Low
Exponential mean	Tunable	Tunable	High	Low
Median / robust filter	Good for isolated spikes	Can suppress impulses	Moderate-high	Low-moderate
Learned temporal encoder	Data-dependent	Potentially high	Lower	High

Strategy	Noise suppression	Transient sensitivity	Interpretability	Deployment burden
Raw + smoothed hybrid	Flexible	Can retain transients	Moderate	Moderate

Table 10 rates six strategies on noise suppression, transient sensitivity, interpretability, and deployment burden. No smoothing preserves transient signals but provides no noise reduction, while moving and exponential means offer moderate to adjustable noise suppression with high interpretability and low implementation burden. Median filters effectively handle isolated spikes but may suppress important impulsive signals, whereas learned temporal encoders are data-dependent, less interpretable, and more computationally demanding. A raw-plus-smoothed hybrid approach provides greater flexibility while retaining transient information, making ablation tests that evaluate the contribution of each channel particularly important (Wu et al., 2024). Furthermore, Wijaya and Sulyono (2025) demonstrated the practical application of machine learning-based damage prediction to support preventive maintenance and improve diagnostic efficiency, reinforcing the importance of evaluating predictive approaches in operational settings.

For operators in Nepal and similar settings, practical constraints may include limited failure histories, mixed-age equipment, intermittent connectivity, and maintenance records maintained on paper or spreadsheets. A low-cost summability stage can operate on an edge gateway during network interruptions; however, consistent sensor identifiers, timestamps, measurement units, maintenance-event codes, and failure definitions remain essential. Imantha et al. (2026) demonstrated how digital material-management systems can improve traceability and operational information management in power-generation facilities, highlighting the importance of structured data management in industrial environments. Implementation should therefore proceed gradually, beginning with a non-safety-critical asset family in shadow mode and comparing predicted warnings with actual inspection findings before integrating estimates into maintenance work orders. This approach is also consistent with Parlindungan et al. (2026), who emphasized preventive maintenance and operational risk mitigation in fuel distribution management. Throughout implementation, statutory inspections and existing protection systems should remain fully operational.

5. Conclusions

5.1 Conclusion

This paper presented a mathematical and operational framework for summability-based remaining useful life estimation, in which noisy causal sensor features are transformed by normalized weighted means before degradation rate or a learned RUL model is estimated. Moving, cumulative and exponential means have distinct memory and responsiveness, which can be described by weight normalization, effective sample size, variance reduction and trend lag. In the pump example a smoothed index of 0.723 gave an RUL of about 61.6 hours that moved to 46.2 or 92.3 hours under modest slope changes, and in the Monte Carlo experiment smoothing cut false first alarms from 78.2% to 0.6% and 2.0% at the cost of a few hours of delay. The most defensible conclusion is conditional: summability is a low-cost, interpretable preprocessing option when noise obscures slow degradation, but it can delay warnings and suppress diagnostic transients, so RUL must remain a decision-support signal integrated with inspection evidence, maintenance policy and engineering judgement.

5.2 Research Limitations

The principal limitation is the absence of a new empirical industrial dataset, since the pump values, Monte Carlo results, IMS replica and ablation values are synthetic and no claim is made that the method outperforms existing algorithms. The local linear threshold model is simple and may fail for nonlinear degradation, change points or partial recovery after maintenance. The threshold is assumed known, although it may depend on manufacturer guidance, standards and plant policy, and further threats include sensor drift, missing-not-at-random data, maintenance-induced distribution shifts, censoring and leakage.

5.3 Suggestions and Directions for Future Research

Future work should investigate regime-aware filters whose memory responds to detected operating regimes through predeclared change-point tests, and should combine summability with quantile regression, Bayesian state-space models or conformal prediction while checking coverage by asset family, mode and horizon. Multi-sensor fusion with sensor-specific filters and physics-informed constraints could reduce implausible RUL oscillations without hiding abrupt faults. A strong benchmark would evaluate C-MAPSS, the IMS and PRONOSTIA bearings and an industrial case under a common protocol, reporting code, filter settings, unit lists, failure definitions, calibration plots and edge latency.

Future industrial deployment should follow a structured, auditable maintenance lifecycle. First, sensor measurements and maintenance logs should be acquired together with data-quality flags. The selected summability filter should then be applied to estimate the degradation trend, Remaining Useful Life (RUL), and its uncertainty interval. Maintenance risk should be assessed by comparing the lower bound of the RUL interval with the required inspection or intervention lead time. Any consequential maintenance action must receive human approval before work orders, spare parts, and schedules are finalized. After inspection or maintenance, outcomes should be recorded and classified as a confirmed fault, no fault found, a sensor issue, or a process transient. These labelled outcomes should inform offline model recalibration, version control, and re-validation before the updated model is returned to operation. Throughout this process, model recommendations must not override protective trips, statutory inspections, or established safety requirements.

Acknowledgement

The authors thank the Faculty of Science, Technology, and Engineering, Rajarshi Janak University, for academic support during the preparation of this study.

References

Ait Mokhtar, E. H., Laggoune, R., & Chateauneuf, A. (2023). Imperfect maintenance modeling and assessment of repairable multi-component systems. *Reliability Engineering & System Safety, 234, 109189*. https://doi.org/10.1016/j.ress.2023.109189

Bai, R., Noman, K., Feng, K., Peng, Z., & Li, Y. (2023). A two-phase-based deep neural network for simultaneous health monitoring and prediction of rolling bearings. *Reliability Engineering & System Safety, 238, 109428*. https://doi.org/10.1016/j.ress.2023.109428

Baranwal, A., Kumar, N., Chatterjee, K., & Koukouvinos, C. (2025). A new EWMA chart for simultaneously monitoring the parameters of a shifted exponential distribution. *Journal of Applied Statistics*, *52*(1), 221-252. https://doi.org/10.1080/02664763.2024.2363404

Betz, W., Papaioannou, I., & Straub, D. (2022). Bayesian post-processing of Monte Carlo simulation in reliability analysis. *Reliability Engineering & System Safety, 227, 108731*. https://doi.org/10.1016/j.ress.2022.108731

Buntinas, M. (2022). *Summability*. United Kingdom: Cambridge University Press.

Chagas, J. Q., Tenreiro Machado, J. A., & Lopes, A. M. (2021). Overview in summabilities: Summation methods for divergent series, Ramanujan summation and fractional finite sums. *Mathematics*, *9*(22), 2963. https://doi.org/10.3390/math9222963

Chen, P., He, C., Hu, X., Yu, D., & Zhang, J. (2025). A comparison of MEWMA and MCUSUM control charts for monitoring bivariate Weibull distribution. *Communications in Statistics: Theory and Methods*, *54*(23), 7630-7650. https://doi.org/10.1080/03610926.2025.2479076

Goebel, K., Saha, B., Saxena, A., Celaya, J. R., & Christophersen, J. P. (2008). Prognostics in battery health management. *IEEE Instrumentation & Measurement Magazine*, *11*(4), 33-40. https://doi.org/10.1109/MIM.2008.4579269

Guo, W., Li, X., & Wan, X. (2023). A novel approach to bearing prognostics based on impulse-driven measures, improved morphological filter and practical health indicator construction. *Reliability Engineering & System Safety, 238, 109451*. https://doi.org/10.1016/j.ress.2023.109451

Hardy, G. H. (1949). *Divergent series*. United Kingdom: Oxford University Press.

Hu, W., Yang, Z., Chen, C., Wu, Y., & Xie, Q. (2021). A Weibull-based recurrent regression model for repairable systems considering double effects of operation and maintenance: A case study of machine tools. *Reliability Engineering & System Safety, 213, 107669*. https://doi.org/10.1016/j.ress.2021.107669

Imantha, D. A., Syahfaj, F. N., Apriyanty, D., & Novalia, N. (2026). SI-MATRE: A no-code integrated application for used material management in a power generation company. *Jurnal Kecerdasan Buatan dan Pembelajaran Mesin*, *1*(1), 35-48. https://doi.org/10.35912/jkbpm.v1i1.6761

ISO. (2022). *Mechanical vibration, measurement and evaluation of machine vibration, Part 3: Industrial machinery with a power rating above 15 kW and operating speeds between 120 r/min and 30 000 r/min (ISO 20816-3:2022)*. Switzerland: International Organization for Standardization.

Jardine, A. K. S., Lin, D., & Banjevic, D. (2006). A review on machinery diagnostics and prognostics implementing condition-based maintenance. *Mechanical Systems and Signal Processing*, *20*(7), 1483-1510. https://doi.org/10.1016/j.ymssp.2005.09.012

Kala, Z. (2022). Quantification of model uncertainty based on variance and entropy of Bernoulli distribution. *Mathematics*, *10*(21), 3980. https://doi.org/10.3390/math10213980

Kartal Erdoğan, B. (2026). Inclusion relations between Abel and Cesàro summability in the interval-valued setting. *AIMS Mathematics*, *11*(9), 30566-30580. https://doi.org/10.3934/math.20261211

Li, G., Wei, J., He, J., Yang, H., & Meng, F. (2023). Implicit Kalman filtering method for remaining useful life prediction of rolling bearing with adaptive detection of degradation stage transition point. *Reliability Engineering & System Safety, 235, 109269*. https://doi.org/10.1016/j.ress.2023.109269

Li, M., Fu, T., & Li, Q. (2025). An adjusted CUSUM-based method for change-point detection in two-phase inverse Gaussian degradation processes. *Mathematics*, *13*(19), 3167. https://doi.org/10.3390/math13193167

Liu, P., & Wang, G. (2022). Minimal repair models with non-negligible repair time. *Reliability Engineering & System Safety, 217, 108046*. https://doi.org/10.1016/j.ress.2021.108046

Nectoux, P., Gouriveau, R., Medjaher, K., Ramasso, E., Chebel-Morello, B., Zerhouni, N., & Varnier, C. (2012). PRONOSTIA: An experimental platform for bearings accelerated degradation tests. Paper presented at In Proceedings of the IEEE International Conference on Prognostics and Health Management. Denver, CO, United States: IEEE.

Nguyen, K. T. P., Medjaher, K., & Gogu, C. (2022). Probabilistic deep learning methodology for uncertainty quantification of remaining useful lifetime of multi-component systems. *Reliability Engineering & System Safety, 222, 108383*. https://doi.org/10.1016/j.ress.2022.108383

Parlindungan, P., Kania, D. D., Silalahi, S. A., Puspita, S. M. R., & Shaliha, F. A. (2026). Evaluating fuel distribution fleet performance using fuzzy AHP and RCA at Integrated Terminal Jakarta. *Annals of Human Resource Management Research*, *6*(3), 387-398. https://doi.org/10.35912/ahrmr.v6.n3.p387-398.2026

Pokharel, J. K., Pahari, N. P., & Sahani, S. K. (2023). Critical analyzing on some new application of almost decreasing sequence to Legendre series associated with [B] sum. *Advances in Nonlinear Variational Inequalities*, *26*(2), 36-40. https://doi.org/10.52783/anvi.v26.253

Putra, D. E., Nawawi, Z., & Jambak, M. I. (2023). Using copper-coated round rod electrodes at various depths in freshwater marshes. *Journal of Multidisciplinary Academic and Practice Studies*, *1*(4), 287-297. https://doi.org/10.35912/jomaps.v1i4.1787

Qiu, H., Lee, J., Lin, J., & Yu, G. (2006). Wavelet filter-based weak signature detection method and its application on rolling element bearing prognostics. *Journal of Sound and Vibration, 289(4-5), 1066-1090*.

Sahani, S. K., & Mishra, L. N. (2021). Degree of approximation of signals by Nörlund summability of derived Fourier series. *The Nepali Mathematical Sciences Report*, *38*(2), 13-19. https://doi.org/10.3126/nmsr.v38i2.42845

Sahani, S. K., & Mishra, V. N. (2023). Degree of approximation of functions by Nörlund summability of double Fourier series. *Mathematical Sciences and Applications E-Notes*, *11*(2), 80-88. https://doi.org/10.36753/mathenot.1008750

Sahani, S. K., Mishra, V. N., & Rathour, L. (2022). On Nörlund summability of double Fourier series. *Open Journal of Mathematical Sciences*, *6*(1), 99-107. https://doi.org/10.30538/oms2022.0180

Si, X.-S., Wang, W., Hu, C.-H., & Zhou, D.-H. (2011). Remaining useful life estimation: A review on the statistical data driven approaches. *European Journal of Operational Research*, *213*(1), 1-14. https://doi.org/10.1016/j.ejor.2010.11.018

Wijaya, A., & Sulyono, S. (2025). K-nearest neighbors based matic motorcycle damage prediction system web application preventive maintenance Bengkel Sahabat Motor. *Jurnal Studi Multidisiplin Ilmu*, *3*(1), 45-57. https://doi.org/10.35912/jasmi.v3i1.6937

Wu, F., Wu, Q., Tan, Y., & Xu, X. (2024). Remaining useful life prediction based on deep learning: A survey. *Sensors*, *24*(11), 3454. https://doi.org/10.3390/s24113454

Xie, F., Castagliola, P., Qiao, Y., Hu, X., & Sun, J. (2022). A one-sided exponentially weighted moving average control chart for time between events. *Journal of Applied Statistics*, *49*(15), 3928-3957. https://doi.org/10.1080/02664763.2021.1967894

Zhan, Y., Kong, Z., Wang, Z., Jin, X., & Xu, Z. (2024). Remaining useful life prediction with uncertainty quantification based on multi-distribution fusion structure. *Reliability Engineering & System Safety, 251, 110383*. https://doi.org/10.1016/j.ress.2024.110383

Zhu, R., Chen, Y., Peng, W., & Ye, Z.-S. (2022). Bayesian deep-learning for RUL prediction: An active learning perspective. *Reliability Engineering & System Safety, 228, 108758*. https://doi.org/10.1016/j.ress.2022.108758

Zio, E. (2022). Prognostics and health management (PHM): Where are we and where do we (need to) go in theory and practice. *Reliability Engineering & System Safety, 218, 108119*. https://doi.org/10.1016/j.ress.2021.108119